Facile Co-precipitation Synthesis of Nanosized MnFe2O4 for Effective Removal of Zn(II) Ions From Aqueous Media

Ahmed Alharbi (ahmedalharbi140@yahoo.com)
Faculty of Applied Science, Umm Al-Qura University
Ahmad A. Alluhaybi
Rabigh College of Science and Arts, King Abdulaziz University
Salwa AlReshaidan
Faculty of Science, King Saud University
Hany M. Youssef
College of Science and Humanities in Al-Kharj, Prince Sattam bin Abdulaziz University

Original Research Full Papers

Keywords: Adsorption, Zn(II) ions, MnFe2O4, Spinel

Posted Date: February 9th, 2021

DOI: https://doi.org/10.21203/rs.3.rs-174931/v1

Abstract

In this work, the spinel nanosized $MnFe_2O_4$ (18.14 nm) was facilely synthesized through the co-precipitation method to study the removal of Zn(II) ions from aqueous media. The fabricated $MnFe_2O_4$ sample was characterized using VSM, XRD, HR-TEM, EDS, FE-SEM, and FT-IR analyses. The principal XRD peaks, which are ascribed to (4 4 0), (3 3 3), (4 2 2), (4 0 0), (2 2 2), (3 1 1), (2 2 0), and (1 1 1) crystal planes, prove the cubic assembly of nanosized manganese ferrite as shown from JCPDS No. 74-2403. The EDS pattern confirmed that the % Wt of Mn, Fe, and O is 24.12, 48.04, and 28.15, respectively. The FE-SEM image confirmed the cubic nature of the surface of $MnFe_2O_4$ nanoparticles which have an average size of 110 nm. The saturation magnetization was 65 emu/g. The impacts of initial pH, concentration of Zn(II) ions, contact time, and temperature on the uptake of Zn(II) ions were accurately investigated. The removal of Zn(II) ions is spontaneous, exothermic, and followed the pseudo-second-order model and the Langmuir isotherm. The maximum adsorption capacity equals 330.03 mg/g.

1. Introduction

The expression “heavy metal” is a description for an assembly of metalloids and metals with a density above 5 g/cm^3 [1]. Also, with the fast expansion of manufacturing like melting, mining, food industry, pigment manufacture, cosmetics, pharmaceuticals, fertilizer productions, galvanizing, and insecticides. The access level of these metals into the water sources has raised and according to the carcinogenicity and toxicity of these metals, the underground and surface water contamination become a worldwide concern. Besides, zinc, as an example of heavy metal such as copper, and iron is essential for our health however an elevated concentration of it is extremely poisonous and risky for health and produce specific diseases as skin irritations, stomach cramps, fever, nausea, anemia, vomiting, and even rapid death [2–6]. Consequently, elimination of elevated concentration of zinc similar additional heavy metals is mandatory and principal, and due to the aforementioned causes, the world health organization (WHO) with an elevated warmth informed an allowed concentration of 300 µg/L for zinc in water [7]. Recently, numerous traditional approaches have been exploited for heavy metals eliminations, for example, ion exchange, electrochemical precipitation, chemical precipitation, adsorption, and reverse osmosis [8–12]. Amongst all of the exploited procedures, due to its operation easiness, low-priced, eco-friendly and elevated efficiency, adsorption is informed as the greatest appropriate approach [13, 14]. So far, there have been exploiting various adsorbents for heavy metals elimination similar zeolites, resins, clay minerals, biosorbents, and several industrial wastes such as fly ash, however, all of them have public characteristics of separation difficulties and little uptake capacities [15–20]. Newly, with the expansion of nanoscience, nanosized substances (typically with the size < 100 nm) due to their distinctive properties such as elevated surface/volume ratio, rich active centers, and elevated uptake capacity, have been respected and have additional application in the recognition and removal of inorganic and organic pollutants. Amongst all nanosized substances, magnetic nanoparticles, besides having the beyond properties, owing to their magnetic characteristics and simple separation with the service of an outer magnet, have been respected more [21–24]. Furthermore, spinel ferrites (Chemical formula: MFe_2O_4) (M

= Mn(II), Fe(II), Zn(II), Co(II), etc.) is additionally a cluster of magnetic nanosized substances which are broadly used in numerous fields such as catalysts, electrical devices and biomedicine, and their distinct properties such as outstanding magnetic characteristics, chemical constancy, elevated particular surface area and fast uptake kinetics have moreover been exploited in the uptake and elimination of the contamination from wastewater [25–28]. The chemical and physical characteristics of spinel ferrites such as magnetic performance depend on the nature of divalent positive ions in addition to the distribution of divalent cation and Fe(III) ions between octahedral and tetrahedral crystallographic locations. In this view, the spinel ferrites categorized into three classes: inverse, normal, and mixed. Also, in the normal kind of spinel, M(II) positive ions take tetrahedral positions entirely, and Fe(III) take octahedral positions such as $ZnFe_2O_4$, whereas in the inverse kind, M(II) positive ions take octahedral positions and Fe(III) take both positions equally such as $CoFe_2O_4$ and Fe_3O_4. In a mixed kind, both positive ions take both positions randomly such as $MnFe_2O_4$ [29, 30]. Recently, the ferrites were utilized more extensively, as the adsorbents of a variety of heavy metals from aqueous media. In these positions, in order to eliminate zinc, bare Fe_3O_4 nanosized particles and Fe_3O_4 with several modifying and coating agents have the maximum usage. For example, Karami fabricate bare Fe_3O_4 through an electrochemical technique (pulsed current) to eliminate several heavy metals containing zinc. According to Karami study, the zinc uptake with magnetite obeyed the pseudo-second-order kinetics and Langmuir isotherm and depend on the Langmuir isotherm, the greatest uptake capacity was 107.70 mg/g [31]. Besides, in additional paper, Bao et al. exploited an amino-functionalized $SiO_2@Fe_3O_4$ magnetic substance for the uptake of Zn(II) ions from pickling waste (hot-dip galvanizing). The magnetic nanosized particles (surface area = 33.70 m^2/g) removed Zn(II) ions by the obeying of Freundlich model with the greatest capacity (169.50 mg/g) at pH 5 [32]. Further Fe_3O_4 nanoparticles such as coated Fe_3O_4 with 3-aminopropyltriethoxysilane alongside two copolymers and Fe_3O_4 modified chitosan were used to eliminate Zn(II) ions. These adsorbents eliminated Zn(II) ions by the obeying of Langmuir model with the greatest uptake capacities of 5.30 and 32.16 mg/g at pH 5.5 and 5, respectively [33]. In this work, because of the elevated magnetization and simple separation of manganese spinel ferrite ($MnFe_2O_4$), the elimination of Zn(II) ions from aqueous solutions was completely studied.

2. Chemicals And Methods

2.1. Chemicals

Entirely the chemical reagents consumed in this paper were of analytical grade (AG) and consumed without additional refining. $ZnCl_2$, $MnCl_2{\cdot}4H_2O$, $FeCl_3{\cdot}6H_2O$, HCl, KOH, H_2SO_4, HNO_3, and CH_3COCH_3 all were bought from Merck company.

2.2. Fabrication of nanosized $MnFe_2O_4$

For the fabrication of nanosized $MnFe_2O_4$ particles, a directly co-precipitation approach was utilized as the following; a particular quantity of $MnCl_2{\cdot}4H_2O$ and $FeCl_3{\cdot}6H_2O$ with a Fe/Mn molar ratio equals 2:1

was dissolved in 130 mL of deionized water under strong stirring and presence of nitrogen gas. Then, the solution was warmed up to 75°C and afterward 7.50 M KOH (was warmed up 75°C before) was added to beyond solution drop by drop with constant stirring, till pH equals 11.22. The mixture kept in that condition for 120 min. Then, the black produced precipitate was magnetically separated at room temperature. Besides, the last precipitate was dried for one day at room temperature after being cleaned with deionized water and acetone numerous times.

2.3. Adsorption tests

The adsorption reactions were accomplished via adding 0.5 g/L nanosized $MnFe_2O_4$ to the flask containing 50 mL of 200 mg/L Zn(II) solution and spinning at 300 rpm. Besides, the adsorption performance of nanosized $MnFe_2O_4$ was studied at different pH values varying from 2.5 to 7.5 for 120 min. The pH was regulated through adding 0.1 M KOH or HCl. The kinetics experiments (uptake time: 10–120 min), the uptake isotherms (Zn(II) concentration: 100–500 mg/L), and the thermodynamics tests (uptake temperature: 298–328 kelvin) were performed, followed by gaining pH equals 6.50. The separation of nanosized $MnFe_2O_4$ was done with a magnet every time.

The subsequent formula is utilized to determine the adsorption capacity (Q, mg/g):

$Q=(C_o-C_e) \times V/m$ (1)

Also, the subsequent formula is utilized to determine the % removal (% R):

$\% R= (C_o-C_e) \times 100/C_o$ (2)

where, C_e (mg/L) and C_o (mg/L) are the final and initial concentrations of Zn(II) ions, respectively. Besides, V (L) is the volume of zinc solution and m (g) is the mass of utilized adsorbent.

2.4. Characterization

Crystal data of nanosized $MnFe_2O_4$ were gotten by X-ray powder diffraction (CuKα radiation with λ equals 0.15 nm). Also, the morphology of nanosized $MnFe_2O_4$ were gotten by a field emission scanning electron microscope alongside with an energy dispersive spectrometer. Besides, the magnetic features of nanosized $MnFe_2O_4$ were studied using a vibrating sample magnetometer at 298 K. Moreover, the Zn(II) concentration was determined via an atomic absorption spectrometer.

3. Results And Discussion

3.1. Characterization of nanosized $MnFe_2O_4$

The XRD pattern of nanosized MFe_2O_4 is presented in Fig. 1. The principal XRD peaks which are ascribed to (4 4 0), (3 3 3), (4 2 2), (4 0 0), (2 2 2), (3 1 1), (2 2 0), and (1 1 1) crystal planes, prove the cubic

assembly of nanosized manganese ferrite (JCPDS No. 74-2403) [34.35]. The average crystallite size of the synthesized manganese ferrite sample estimated via the subsequent Scherrer equation is 18.14 nm:

Crystallite size (nm) = Kλ/βcosθ

Where, K is the Scherrer constant, β is the full width at half-maximum of XRD peaks, λ is the wavelength of KαCu radiation, and θ is the diffraction angle. Figure 2 shows the EDS analysis of nanosized $MnFe_2O_4$ sample. The results show that the % Wt of Mn, Fe, and O is 24.12, 48.04, and 28.15, respectively. The surface morphology using FE-SEM for nanosized $MnFe_2O_4$ is displayed in Fig. 3. The results confirmed the cubic nature of the surface of $MnFe_2O_4$ nanoparticles which have an average size of 110 nm. Figure 4 shows the HR-TEM image of nanosized $MnFe_2O_4$ sample. The results confirmed that the sample consist of sphere and irregular shapes with an average diameter of 15.93 nm. Construction of the spinel nanosized $MnFe_2O_4$ was further confirmed using FT-IR analysis. Figure 5 presents the FT-IR spectrum of nanosized $MnFe_2O_4$. The spectra display two principal bands below 1000 cm^{-1} which is a familiar characteristic of ferrites. These characteristic bands at 575 and 450 cm^{-1} attributed to essential stretching vibrations of the oxygen-metal at the tetrahedral and octahedral sites, respectively. The bands which were observed at 1635 and 3370 cm^{-1} are due to stretching and bending vibration of adsorbed water, respectively [36–45]. The magnetization curve of the nanosized $MnFe_2O_4$ is displayed in Fig. 6. The results prove the superparamagnetic performance of the synthesized sample. Also, the saturation magnetization for nanosized $MnFe_2O_4$ is 65 emu/g which is considered more than 16.3 emu/g (Minimum required saturation for magnetic separation from aqueous media with an external magnet).

3.2. Adsorption of Zn(II) ions from aqueous media

The relation between adsorption pH and % removal of Zn(II) ions using nanosized $MnFe_2O_4$ is displayed in Fig. 7A. Also, the relation between adsorption pH and the quantity of adsorbed Zn(II) ions with nanosized $MnFe_2O_4$ is displayed in Fig. 7B. The results confirmed that the % removal of Zn(II) ions and the quantity of adsorbed Zn(II) ions improved via increasing pH until equals 78.5 % and 314 mg/g, respectively at the optimum pH which equals 6.5.

The relation between adsorption time and % removal of Zn(II) ions using nanosized $MnFe_2O_4$ is displayed in Fig. 8A. Also, the relation between adsorption time and the quantity of adsorbed Zn(II) ions with nanosized $MnFe_2O_4$ is displayed in Fig. 8B. The results confirmed that the % removal of Zn(II) ions and the quantity of adsorbed Zn(II) ions improved via increasing time until equals 77.5 % and 310 mg/g, respectively at the optimum time which equals 60 min.

The adsorption kinetics was examined via pseudo-first-order (Fig. 9A) and, pseudo-second-order (Fig. 9B) models, which are donated as Eqs. (3) and (4), respectively [36–45]:

$\log (Q_e - Q_t) = \log Q_e - K_1 t/2.303$ (3)

$t/Q_t = (1/K_2Q_e^2) + (1/Q_e)\ t$ (4)

where, Q_t (mg/g) is the amount of adsorbed Zn(II) ions at time t whereas Q_e (mg/g) is the amount of adsorbed Zn(II) ions at equilibrium. Also, K_2 (g/mg.min) is the pseudo-second-order rate constant whereas K_1 (1/min) term is the pseudo-first-order rate constant. The data of pseudo-first-order and pseudo-second-order kinetics models are displayed in Table 1. Owing to the greater correlation coefficient (R^2) of pseudo-second-order and the small alterations between the calculated and experimental adsorption capacity by pseudo-second-order, the adsorption of Zn(II) ions follows the pseudo-second-order kinetic model.

Table 1
Kinetic constants

Pseudo first order			**Pseudo second order**		
Q (mg/g)	K_F (1/min)	R^2	Q (mg/g)	K_S (g/mg.min)	R^2
260.68	0.034	0.994	364.96	0.0001	0.999

The relation between primary concentration and % removal of Zn(II) ions using nanosized $MnFe_2O_4$ is displayed in Fig. 10A. Also, the relation between primary concentration and the quantity of adsorbed Zn(II) ions with nanosized $MnFe_2O_4$ is displayed in Fig. 10B. The results confirmed that the % removal of Zn(II) ions decreased while the quantity of adsorbed Zn(II) ions improved via increasing primary concentration. The adsorption isotherm is an appreciated relation that explains the behavior of adsorption equilibrium between a solid-phase and adsorbate at a constant pH and temperature. The Langmuir (single-layer adsorption) (Fig. 11A) and Freundlich (multi-layer adsorption) (Fig. 11B) isotherms were estimated in this work as denoted in Eqs. (4) and (5), respectively [36–45].

$\ln Q_e = \ln K_F + (1/n)\ \ln C_e$ (4)

$C_e/Q_e = (1/K_LQ_m) + (C_e/Q_m)$ (5)

where, Q_m (mg/g) is the maximum Langmuir adsorption capacity while K_L (L/mg) is the Langmuir constant. Further, K_F (mg/g)(L/mg)$^{1/n}$ is the Freundlich constant whereas 1/n is the heterogeneity factor. Furthermore, the Q_m of Freundlich isotherm was estimated via Eq. (6).

$Q_m = K_F\ (C_o)^{\ 1/n}$ (6)

The data of Langmuir and Freundlich kinetics models are displayed in Table 2.

Table 2
Equilibrium constants

Langmuir			Freundlich		
Q (mg/g)	K_L (L/mg)	R^2	Q (mg/g)	K_F (mg/g)(L/mg)$^{1/n}$	R^2
330.03	0.423	0.999	323.92	226.19	0.971

Owing to the elevated correlation coefficient of Langmuir isotherm (R_L^2), the adsorption happens for $MnFe_2O_4$ and the maximum adsorption capacity equals 330.03 mg/g.

The relation between adsorption temperature and % removal of Zn(II) ions using nanosized $MnFe_2O_4$ is displayed in Fig. 12A. Also, the relation between adsorption temperature and the quantity of adsorbed Zn(II) ions with nanosized $MnFe_2O_4$ is displayed in Fig. 12B. The results confirmed that the % removal of Zn(II) ions and the quantity of adsorbed Zn(II) ions decreased via increasing temperature. The thermodynamics findings were carried out to examine the spontaneous and feasibility of the adsorption as denoted in Eqs. (7) and (8), respectively [36–45].

$$\ln K_d = (\Delta S^o/R) - (\Delta H^o/RT) \quad (7)$$

$$\Delta G^o = \Delta H^o - T\Delta S^o \quad (8)$$

where, R (KJ/mol K) is the gas constant while T (Kelvin) is the temperature. Also, ΔG^o is the Gibbs free energy change while ΔH^o is the enthalpy change. Further, ΔS^o is the entropy change. Distribution co-efficient (K_d, L/g) can be estimated via Eq. (9)

$$K_d = [\%\ R/\ (100-\%\ R)]\ V/m \quad (9)$$

Figure 12C represents the plot of ln Kd vs. 1/T. The data of thermodynamic parameters are listed in Table 3.

Table 3
Thermodynamic constants

ΔG^o (KJ/mol)				ΔS^o (KJ/molK)	ΔH^o (KJ/mol)
Temperature (Kelvin)					
298	308	318	328		
-27.90	-28.29	-28.68	-29.07	0.039	-16.344

The negativity of enthalpy elucidates the exothermic nature of adsorption of Zn(II) ions while the negativity of Gibbs free energy displays the spontaneous and feasibility adsorption. The Gibbs free energy values reduce by growing the temperature from 298 K to 328 K, which show the beneficial adsorption of Zn(II) ions using $MnFe_2O_4$ at room temperature, as compared with elevated temperatures. The physical adsorption was the prevailing as the ΔH^o value is less than 40 kJ/mol.

Lastly, as seen in Table 4, via comparing the maximum uptake capacity of nanosized $MnFe_2O_4$ with other adsorbents, it can be decided that the current adsorbent is the most operative adsorbent utilized for the removal of Zn(II) ions from aqueous media [31, 32, 46–48].

Table 4
comparison between adsorption capacity of MnFe2O4 and other adsorbents

Adsorbent	Adsorption capacity (mg g^{-1})	Ref
Clinoptilolite	8.70	[46]
Magnetite	107.70	[31]
Fe_3O_4@SiO_2	169.50	[32]
MnO_2	54.50	[33]
Hydroxyapatite	37.50	[47]
$MnFe_2O_4$	330.03	**This study**

4. Conclusions

The cubical nanosized manganese ferrite (18.14 nm) was facilely synthesized via co-precipitation method. The nanosized $MnFe_2O_4$ sample could uptake Zn(II) ions with adsorption capacity equals 330.03 mg/g. The removal of Zn(II) ions was fitted with the Langmuir isotherm and pseudo-second-order kinetic model. Besides, the removal was exothermic, physical, and spontaneous.

Declarations

Conflict of Interest

The authors declare that there is no conflict of interest for this paper.

Acknowledgments

The authors would like to thank the Deanship of Scientific Research at Umm Al-Qura University for supporting this work by Grant Code: (20UQU0063DSR).

References

1. M.A. Hashim, S. Mukhopadhyay, J.N. Sahu, B. Sengupta, Remediation technologies for heavy metal contaminated groundwater, J. Environ. Manage. 92 (2011) 2355–2388.
2. C.F. Carolin, P.S. Kumar, A. Saravanan, G.J. Joshiba, M. Naushad, Efficient techniques for the removal of toxic heavy metals from aquatic environment: A review, J. Environ. Chem. Eng. 5 (2017) 2782–2799.
3. L. Fan, C. Luo, Z. Lv, F. Lu, H. Qiu, Preparation of magnetic modified chitosan and adsorption of Zn^{2+} from aqueous solutions, Colloids Surf. B 88 (2011) 574–581.
4. W.W. Ngah, M. Hanafiah, Removal of heavy metal ions from wastewater by chemically modified plant wastes as adsorbents: a review, Bioresour. Technol. 99 (2008) 3935–3948.
5. F. Fu, Q. Wang, Removal of heavy metal ions from wastewaters: a review, J.Environ. Manage. 92 (2011) 407–418.
6. W. Qiu, Y. Zheng, Removal of lead, copper, nickel, cobalt, and zinc from water by a cancrinite-type zeolite synthesized from fly ash, Chem. Eng. J. 145 (2009) 483–488.
7. F. Edition, Guidelines for drinking-water quality, WHO chronicle 38 (2011)104–108.
8. M. Fazlzadeh, K. Rahmani, A. Zarei, H. Abdoallahzadeh, F. Nasiri, R. Khosravi, A novel green synthesis of zero valent iron nanoparticles (NZVI) using three plant extracts and their efficient application for removal of Cr(VI) from aqueous solutions, Adv. Powder Technol. 28 (2017) 122–130.
9. H. Ozaki, K. Sharma, W. Saktaywin, Performance of an ultra-low-pressure reverse osmosis membrane (ULPROM) for separating heavy metal: effects of interference parameters, Desalination 144 (2002) 287–294.
10. M.M. Matlock, B.S. Howerton, D.A. Atwood, Chemical precipitation of heavy metals from acid mine drainage, Water Res. 36 (2002) 4757–4764.
11. M. Hunsom, K. Pruksathorn, S. Damronglerd, H. Vergnes, P. Duverneuil, Electrochemical treatment of heavy metals (Cu^{2+}, Cr^{6+}, Ni^{2+}) from industrial effluent and modeling of copper reduction, Water Res. 39 (2005) 610–616.
12. A. Da ¸browski, Z. Hubicki, P. Podkos´cielny, E. Robens, Selective removal of the heavy metal ions from waters and industrial wastewaters by ion-exchange method, Chemosphere 56 (2004) 91–106.
13. G. Crini, Recent developments in polysaccharide-based materials used as adsorbents in wastewater treatment, Prog. Polym. Sci. 30 (2005) 38–70.
14. W. Peng, H. Li, Y. Liu, S. Song, A review on heavy metal ions adsorption from water by graphene oxide and its composites, J. Mol. Liq. 230 (2017) 496–504.
15. A. Roy, J. Bhattacharya, Removal of Cu(II), Zn(II) and Pb(II) from water using microwave-assisted synthesized maghemite nanotubes, Chem. Eng. J. 211 (2012) 493–500.
16. M. Visa, C. Bogatu, A. Duta, Simultaneous adsorption of dyes and heavy metals from multicomponent solutions using fly ash, Appl. Surf. Sci. 256 (2010) 5486–5491.

17. H.T. Kahraman, E. Pehlivan, Cr^{6+} removal using oleaster (Elaeagnus) seed and cherry (Prunus avium) stone biochar, Powder Technol. 306 (2017) 61–67.
18. S. Edebali, E. Pehlivan, Evaluation of chelate and cation exchange resins to remove copper ions, Powder Technol. 301 (2016) 520–525.
19. Y. Chu, M.A. Khan, F. Wang, M. Xia, W. Lei, S. Zhu, Kinetics and equilibrium isotherms of adsorption of Pb(II) and Cu(II) onto raw and arginine-modified montmorillonite, Adv. Powder Technol. 30 (2019) 1067–1078.
20. M. Visa, Synthesis and characterization of new zeolite materials obtained from fly ash for heavy metals removal in advanced wastewater treatment, Powder Technol. 294 (2016) 338–347.
21. A.K. Gupta, M. Gupta, Synthesis and surface engineering of iron oxide nanoparticles for biomedical applications, Biomaterials 26 (2005) 3995–4021.
22. I. Ali, New generation adsorbents for water treatment, Chem. Rev. 112 (2012) 5073–5091.
23. H.L. Fan, S.F. Zhou, W.Z. Jiao, G.S. Qi, Y.Z. Liu, Removal of heavy metal ions by magnetic chitosan nanoparticles prepared continuously via high-gravity reactive precipitation method, Carbohydr. Polym. 174 (2017) 1192–1200.
24. F. Lu, D. Astruc, Nanomaterials for removal of toxic elements from water, Coord. Chem. Rev. 356 (2018) 147–164.
25. K.K. Kefeni, T.A. Msagati, B.B. Mamba, Ferrite nanoparticles: synthesis, characterisation and applications in electronic device, Mater. Sci. Eng. B 215 (2017) 37–55.
26. C. Xu, S. Sun, New forms of superparamagnetic nanoparticles for biomedical applications, Adv. Drug Deliv. Rev. 65 (2013) 732–743.
27. E. Casbeer, V.K. Sharma, X.Z. Li, Synthesis and photocatalytic activity of ferrites under visible light: a review, Sep. Purif. Technol. 87 (2012) 1–14.
28. M.B. Gawande, Y. Monga, R. Zboril, R.K. Sharma, Silica-decorated magnetic nanocomposites for catalytic applications, Coord. Chem. Rev. 288 (2015) 118–143.
29. D.H.K. Reddy, Y.S. Yun, Spinel ferrite magnetic adsorbents: alternative future materials for water purification?, Coord. Chem. Rev 315 (2016) 90–111.
30. K.K. Kefeni, B.B. Mamba, T.A. Msagati, Application of spinel ferrite nanoparticles in water and wastewater treatment: a review, Sep. Purif.Technol. 188 (2017) 399–422.
31. H. Karami, Heavy metal removal from water by magnetite nanorods, Chem.Eng. J. 219 (2013) 209–216.
32. S. Bao, L. Tang, K. Li, P. Ning, J. Peng, H. Guo, T. Zhu, Y. Liu, Highly selective removal of Zn(II) ion from hot-dip galvanizing pickling waste with aminofunctionalized Fe_3O_4@SiO_2 magnetic nano-adsorbent, J. Colloid interface. Sci. 462 (2016) 235–242.
33. F. Ge, M.M. Li, H. Ye, B.X. Zhao, Effective removal of heavy metal ions Cd^{2+}, Zn^{2+}, Pb^{2+}, Cu^{2+} from aqueous solution by polymer-modified magnetic nanoparticles, J. Hazard. Mater. 211 (2012) 366–372.

34. W. Wang, Z. Ding, M. Cai, H. Jian, Z. Zeng, F. Li, J.P. Liu, Synthesis and high efficiency methylene blue adsorption of magnetic PAA/$MnFe_2O_4$ nanocomposites, Appl. Surf. Sci. 346 (2015) 348–353.
35. A.B. Salunkhe, V.M. Khot, M.R. Phadatare, N.D. Thorat, R.S. Joshi, H.M. Yadav, S.H. Pawar, Low temperature combustion synthesis and magnetostructural properties of Co–Mn nanoferrites, J. Magn. Magn. Mater. 352 (2014) 91–98.
36. E.A. Abdelrahman, R.M. Hegazey, R.E. El-Azabawy, Efficient removal of methylene blue dye from aqueous media using Fe/Si, Cr/Si, Ni/Si, and Zn/Si amorphous novel adsorbents, J. Mater. Res. Technol. 8 (2019) 5301–5313.
37. E.A. Abdelrahman, R.M. Hegazey, Exploitation of Egyptian insecticide cans in the fabrication of Si/Fe nanostructures and their chitosan polymer composites for the removal of Ni(II), Cu(II), and Zn(II) ions from aqueous solutions, Compos. Part B Eng. 166 (2019) 382–400.
38. E.A. Abdelrahman, R.M. Hegazey, Utilization of waste aluminum cans in the fabrication of hydroxysodalite nanoparticles and their chitosan biopolymer composites for the removal of Ni(II) and Pb(II) ions from aqueous solutions: Kinetic, equilibrium, and reusability studies, Microchem. J. 145 (2019) 18–25.
39. E.A. Abdelrahman, Synthesis of zeolite nanostructures from waste aluminum cans for efficient removal of malachite green dye from aqueous media, J. Mol. Liq. 253 (2018) 72–82.
40. E.A. Abdelrahman, A. Subaihi, Application of Geopolymers Modified with Chitosan as Novel Composites for Efficient Removal of Hg(II), Cd(II), and Pb(II) Ions from Aqueous Media, J. Inorg. Organomet. Polym. Mater. (2019) Doi:10.1007/s10904-019-01380-0.
41. A.M. Hameed, A. Alharbi, E.A. Abdelrahman, E.M. Mabrouk, R.M. Hegazey, F.K. Algethami, Y.O. Al-Ghamdi, H.M. Youssef, Facile Hydrothermal Fabrication of Analcime and Zeolite X for Efficient Removal of Cd(II) Ions From Aqueous Media and Polluted Water, J. Inorg. Organomet. Polym. Mater. (2020) Doi:10.1007/s10904-020-01565-y.
42. E.A. Abdelrahman, R.M. Hegazey, A. Alharbi, Facile Synthesis of Mordenite Nanoparticles for Efficient Removal of Pb(II) Ions from Aqueous Media, J. Inorg. Organomet. Polym. Mater. 30 (2020) 1369–1383.
43. E.A. Abdelrahman, E.T. Abdel-Salam, S.M. El Rayes, N.S. Mohamed, Facile synthesis of graft copolymers of maltodextrin and chitosan with 2-acrylamido-2-methyl-1-propanesulfonic acid for efficient removal of Ni(II), Fe(III), and Cd(II) ions from aqueous media, J. Polym. Res. 26 (2019) Doi:10.1007/s10965-019-1920-4.
44. A.M. Hameed, Synthesis of Si/Cu Amorphous Adsorbent for Efficient Removal of Methylene Blue Dye from Aqueous Media, J. Inorg. Organomet. Polym. Mater. (2020) Doi:10.1007/s10904-019-01436-1.
45. U. Habiba, T.A. Siddique, T.C. Joo, A. Salleh, B.C. Ang, A.M. Afifi, Synthesis of chitosan/polyvinyl alcohol/zeolite composite for removal of methyl orange, Congo red and chromium(VI) by flocculation/adsorption, Carbohydr. Polym. 157 (2017) 1568–1576.
46. E. Erdem, N. Karapinar, R. Donat, The removal of heavy metal cations by natural zeolites, J. Colloid Interface Sci. 280 (2004) 309–314.

47. Q. Su, B. Pan, S. Wan, W. Zhang, L. Lv, Use of hydrous manganese dioxide as a potential sorbent for selective removal of lead, cadmium, and zinc ions from water, J. Colloid Interface Sci. 349 (2010) 607–612.
48. B. Keochaiyom, J. Wan, G. Zeng, D. Huang, W. Xue, L. Hu, C. Huang, C. Zhang, M. Cheng, Synthesis and application of magnetic chlorapatite nanoparticles for zinc(II), cadmium(II) and lead(II) removal from water solutions, J. Colloid Interface Sci. 505 (2017) 824–835.

Figures

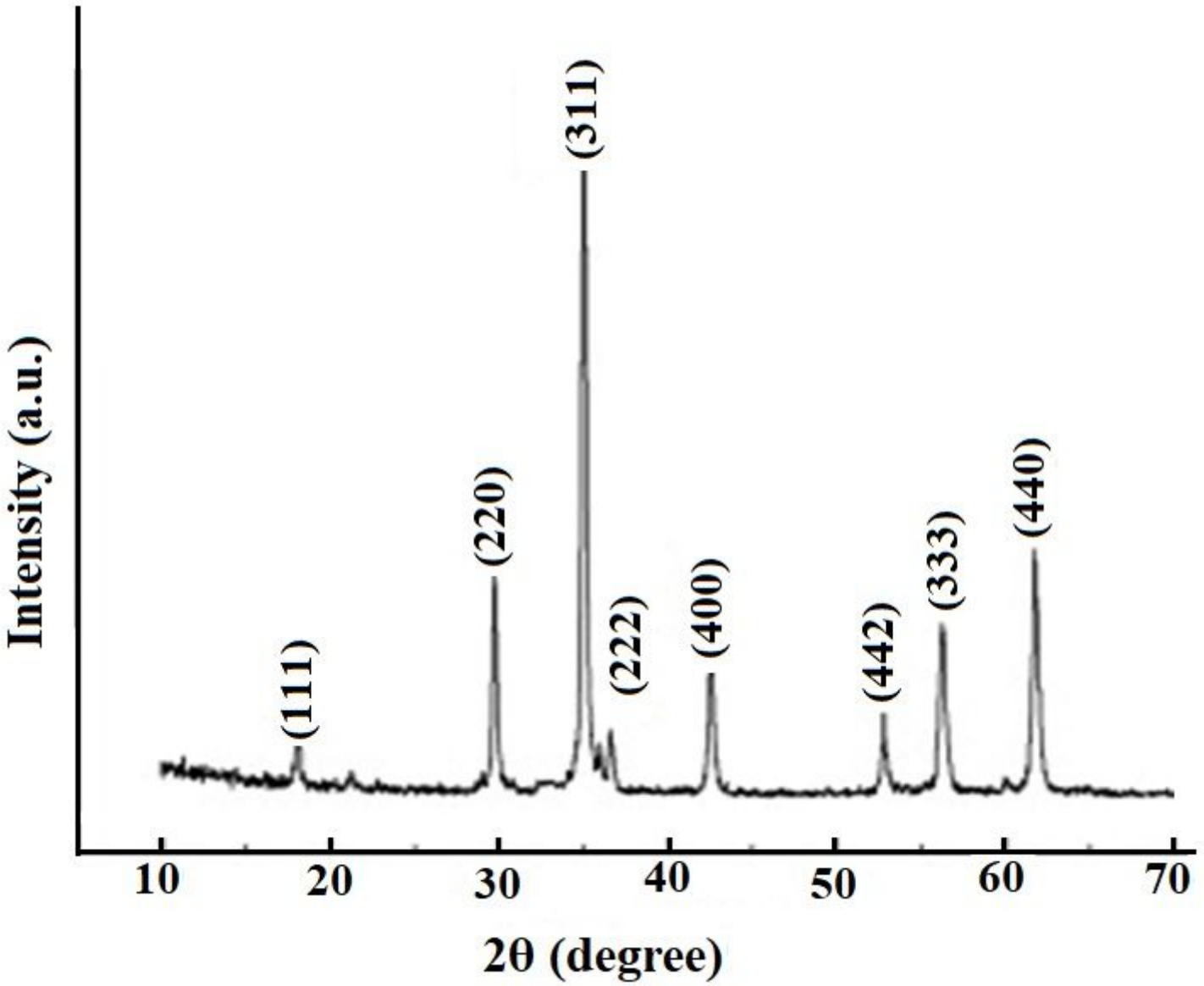

Figure 1

XRD of MnFe2O4 sample

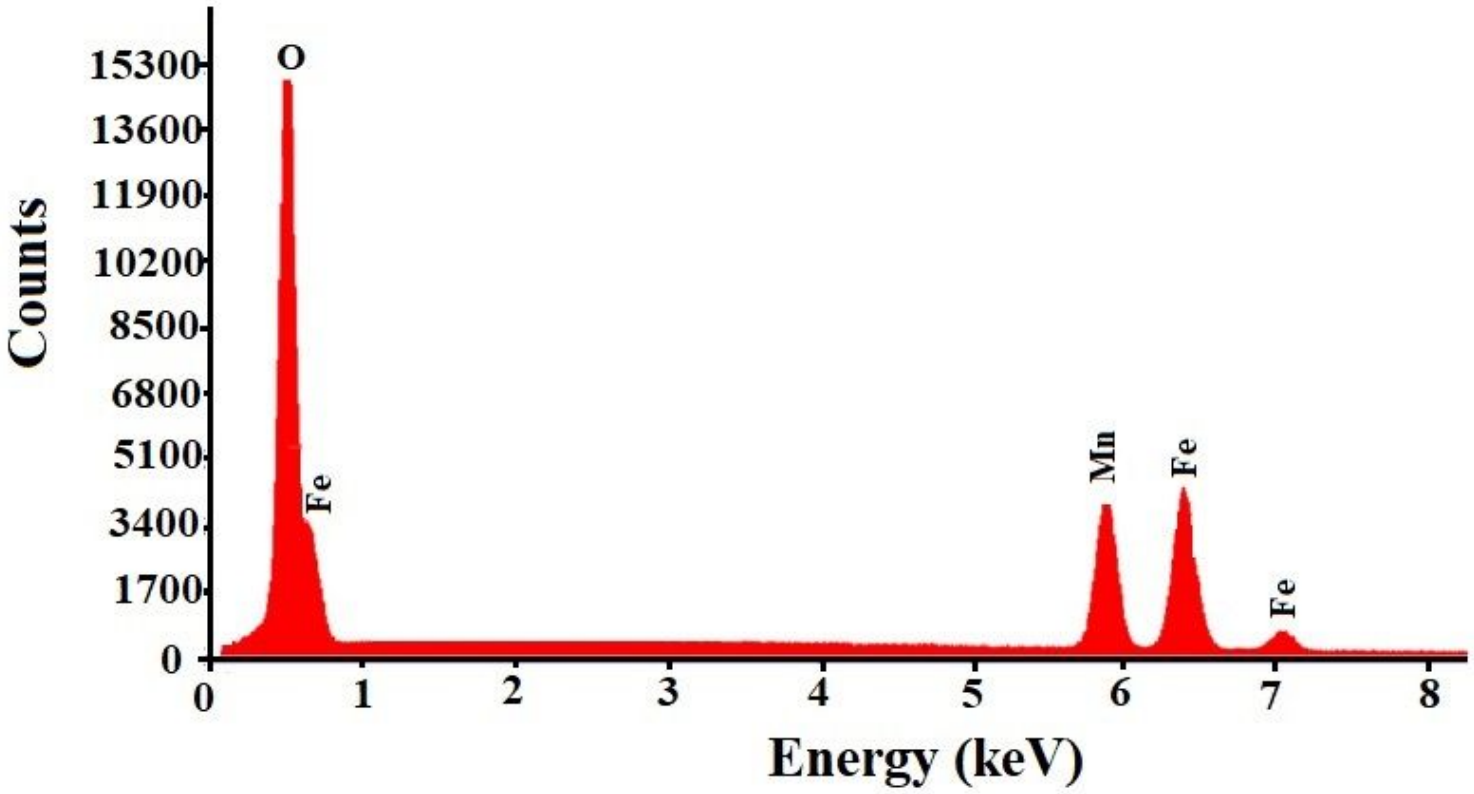

Figure 2

EDS of MnFe2O4 sample

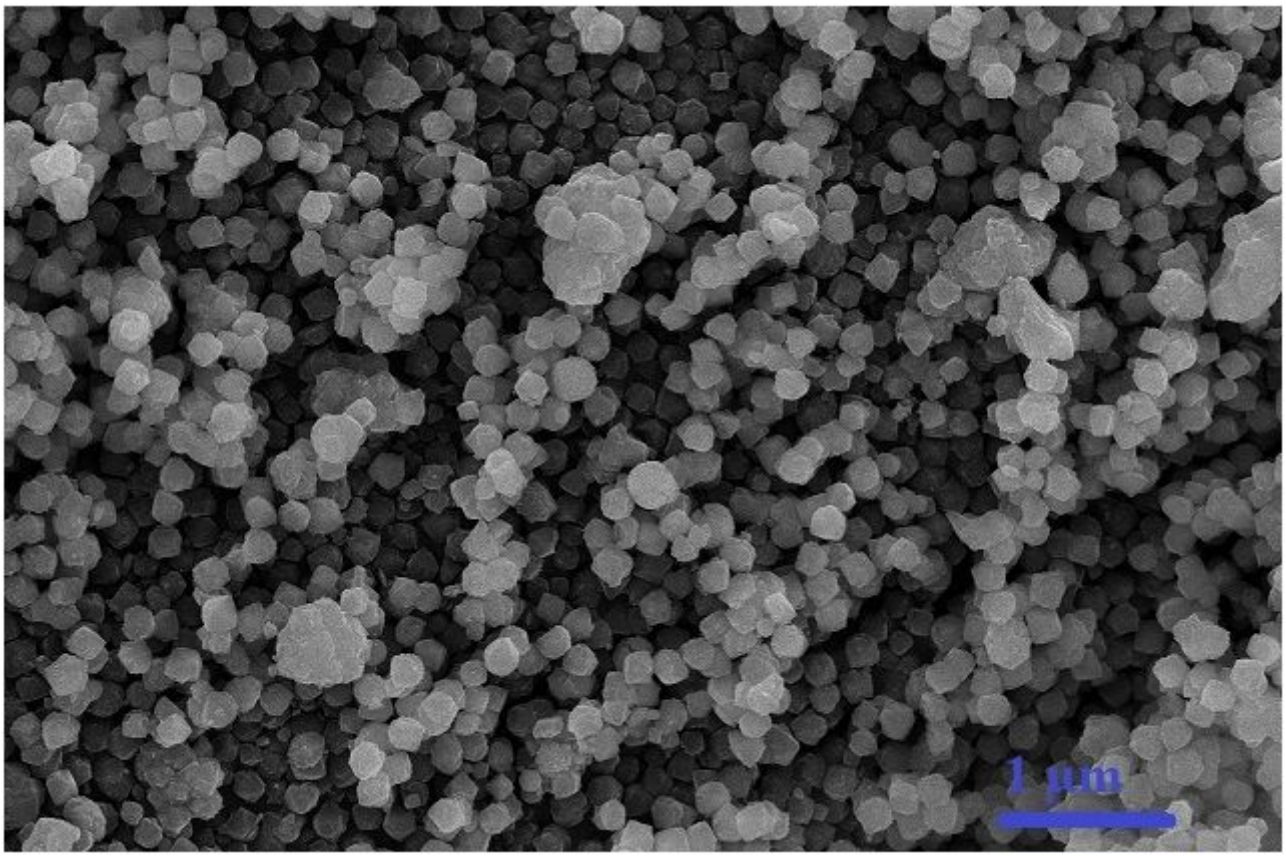

Figure 3

FE-SEM image of MnFe2O4 sample

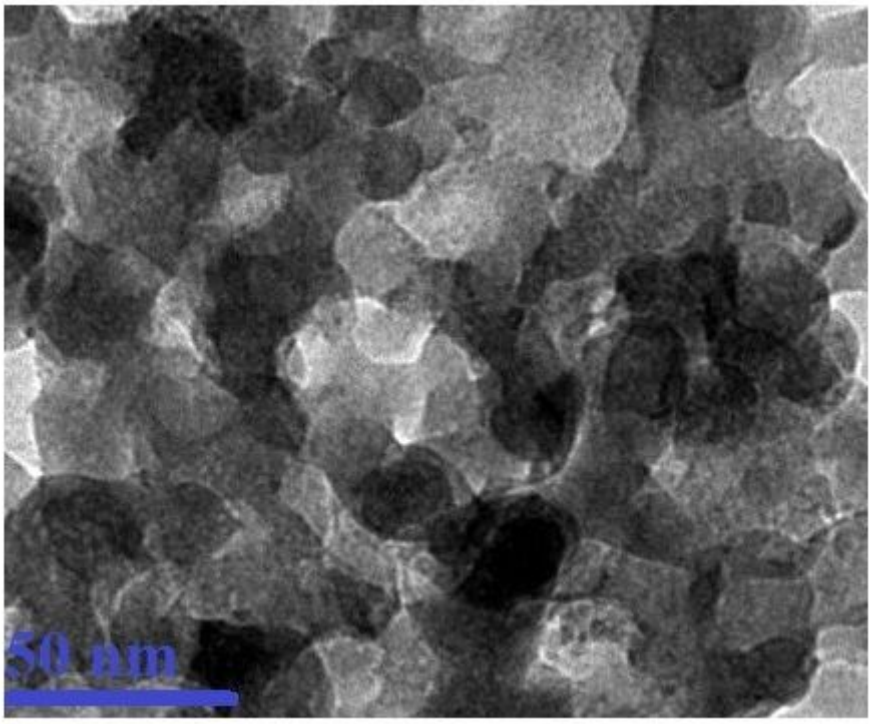

Figure 4

HR-TEM image of MnFe2O4 sample

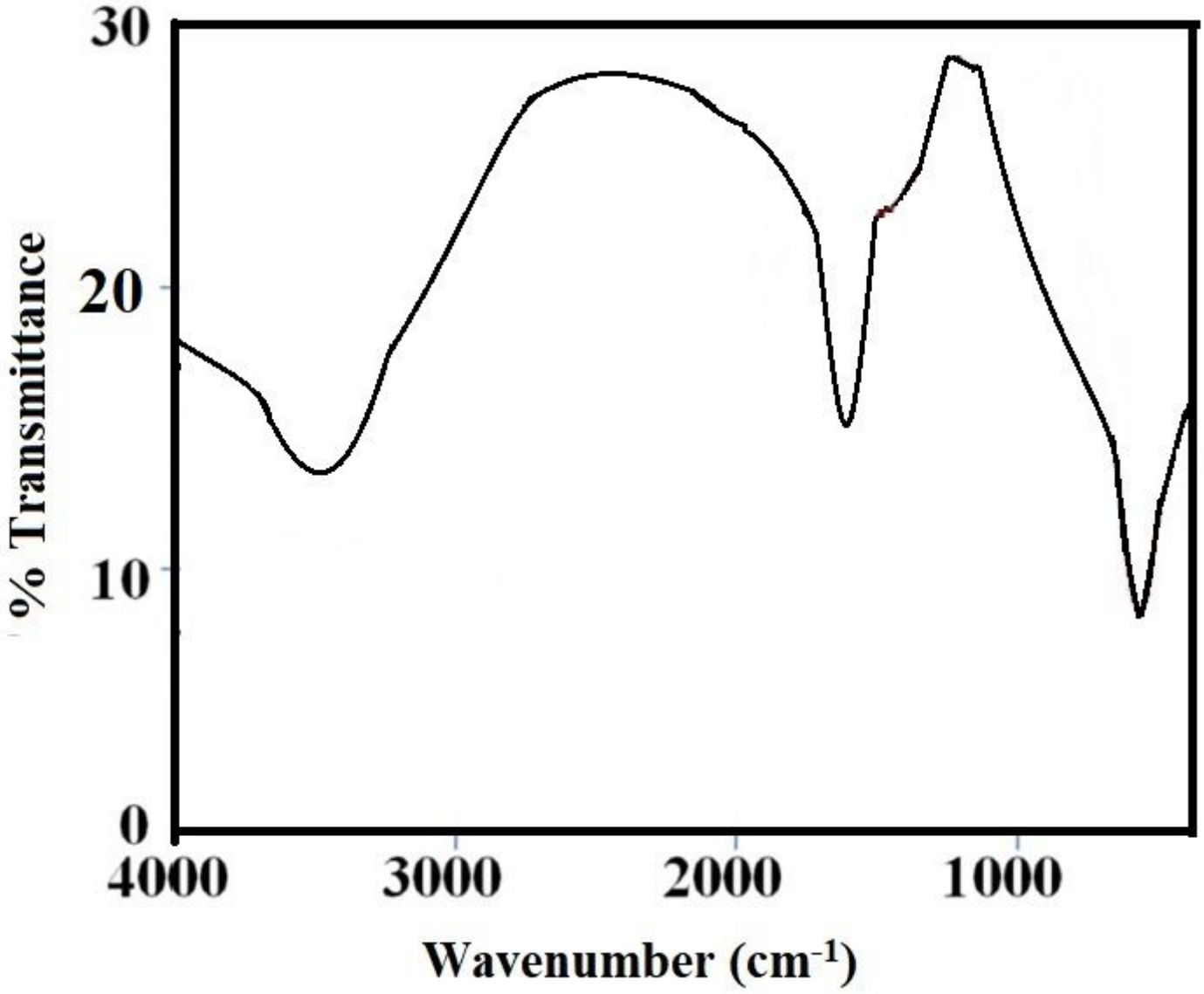

Figure 5

FT-IR of MnFe2O4 sample

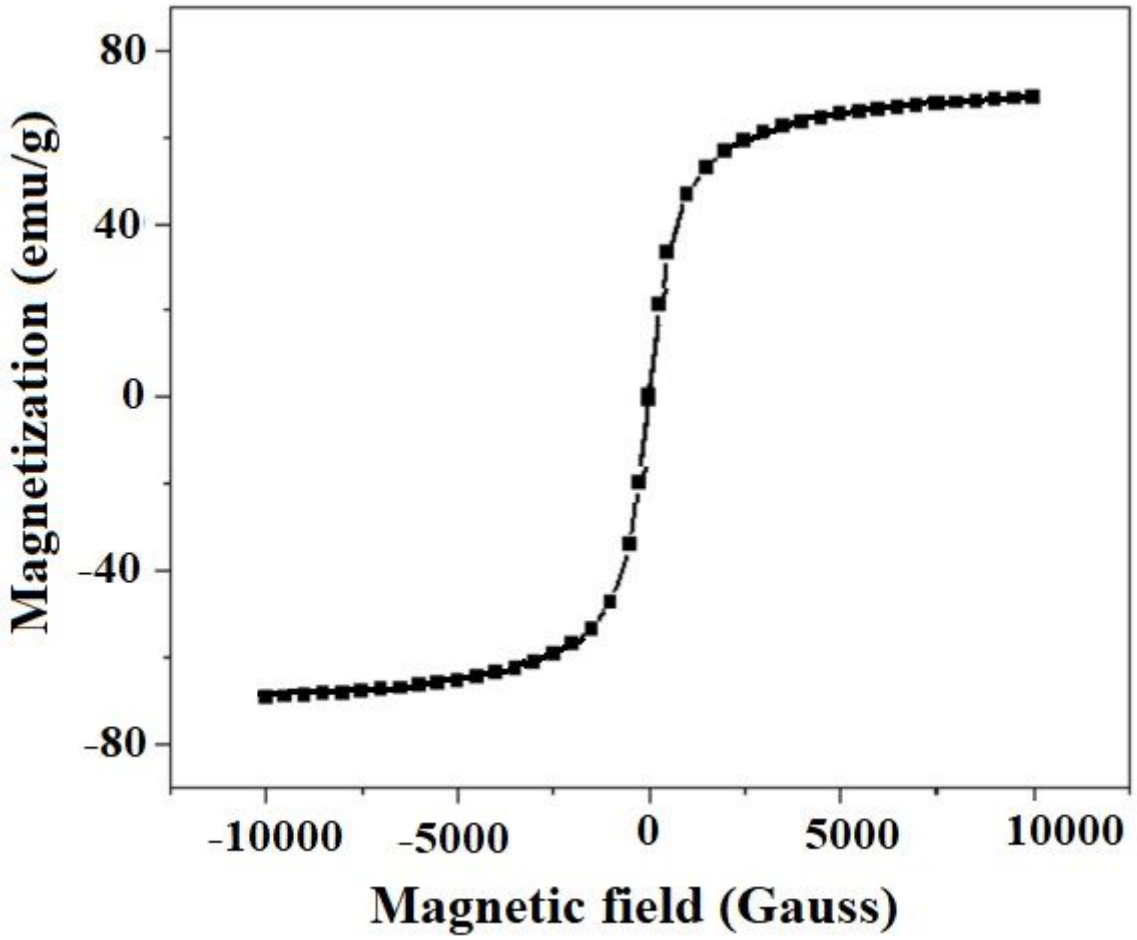

Figure 6

Magnetic properties of MnFe2O4 sample

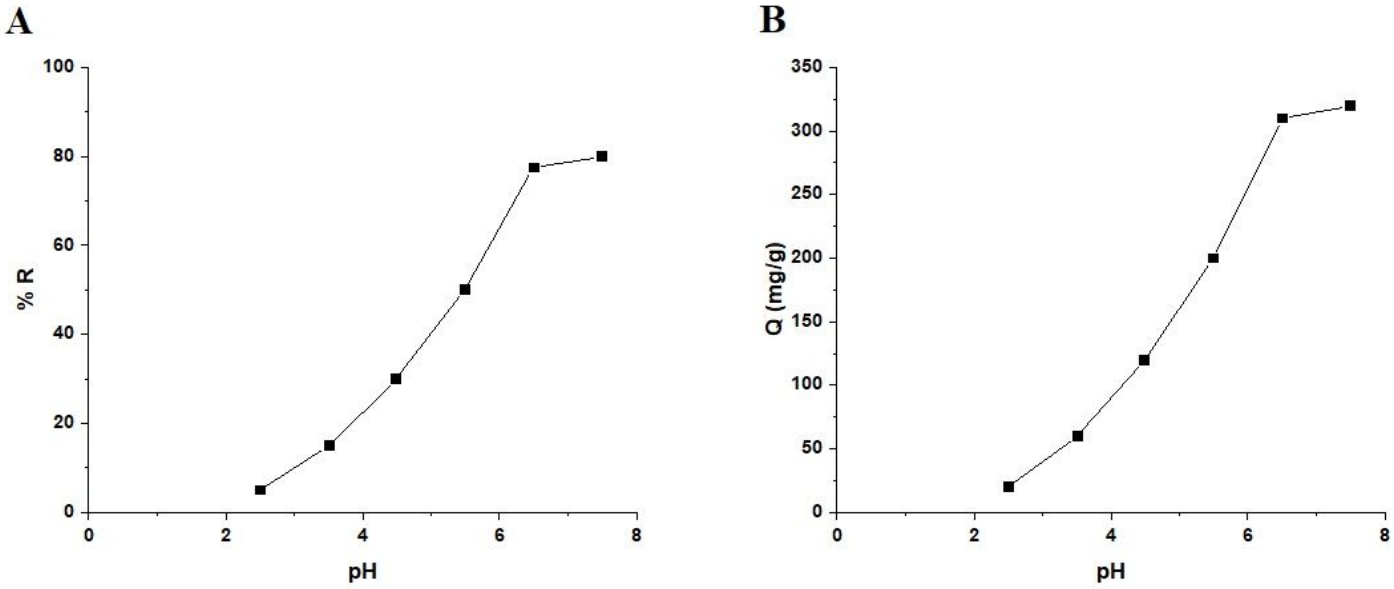

Figure 7

The relation between pH vs. % removal (A) and capacity (B).

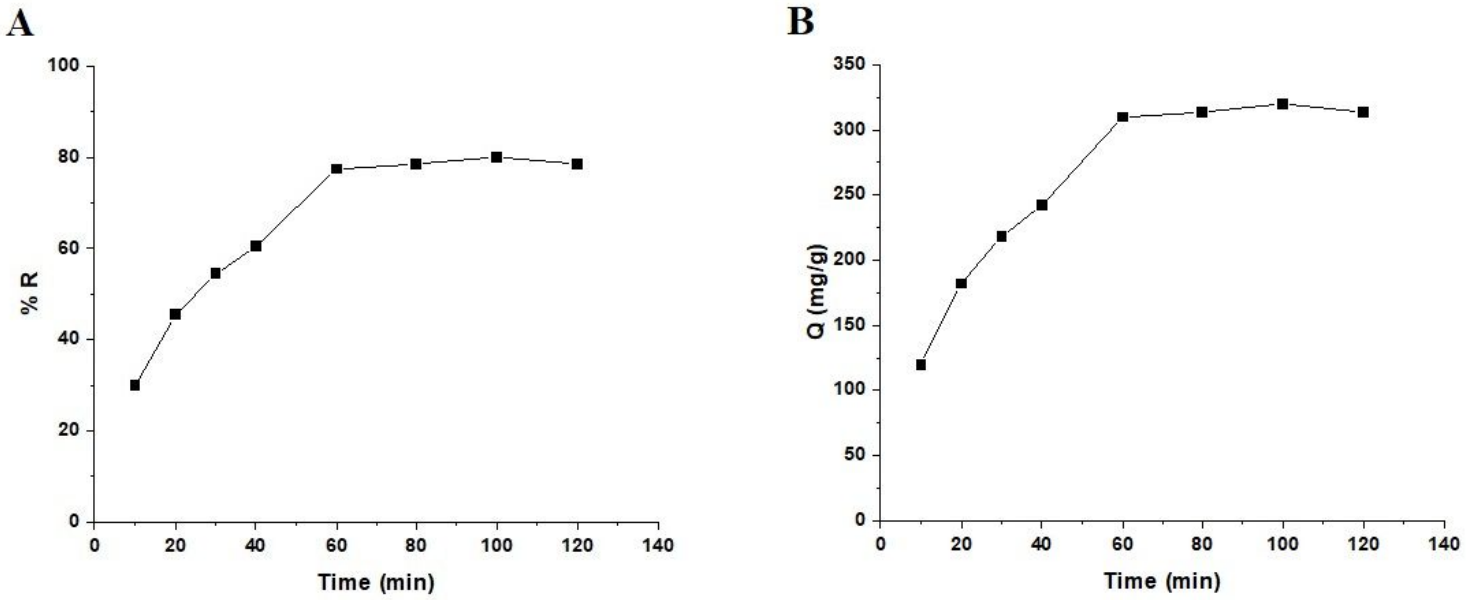

Figure 8

The relation between time vs. % removal (A) and capacity (B).

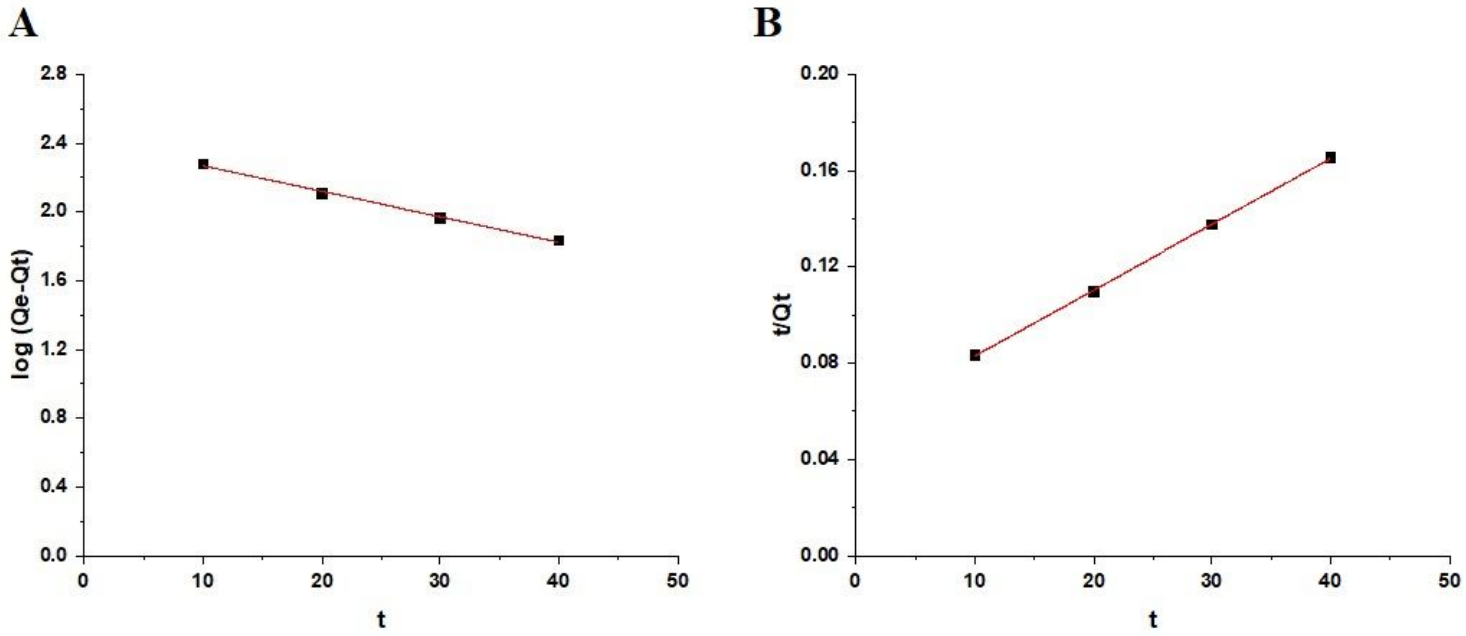

Figure 9

Pseudo-first-order (A) and pseudo-second-order (B) kinetic models.

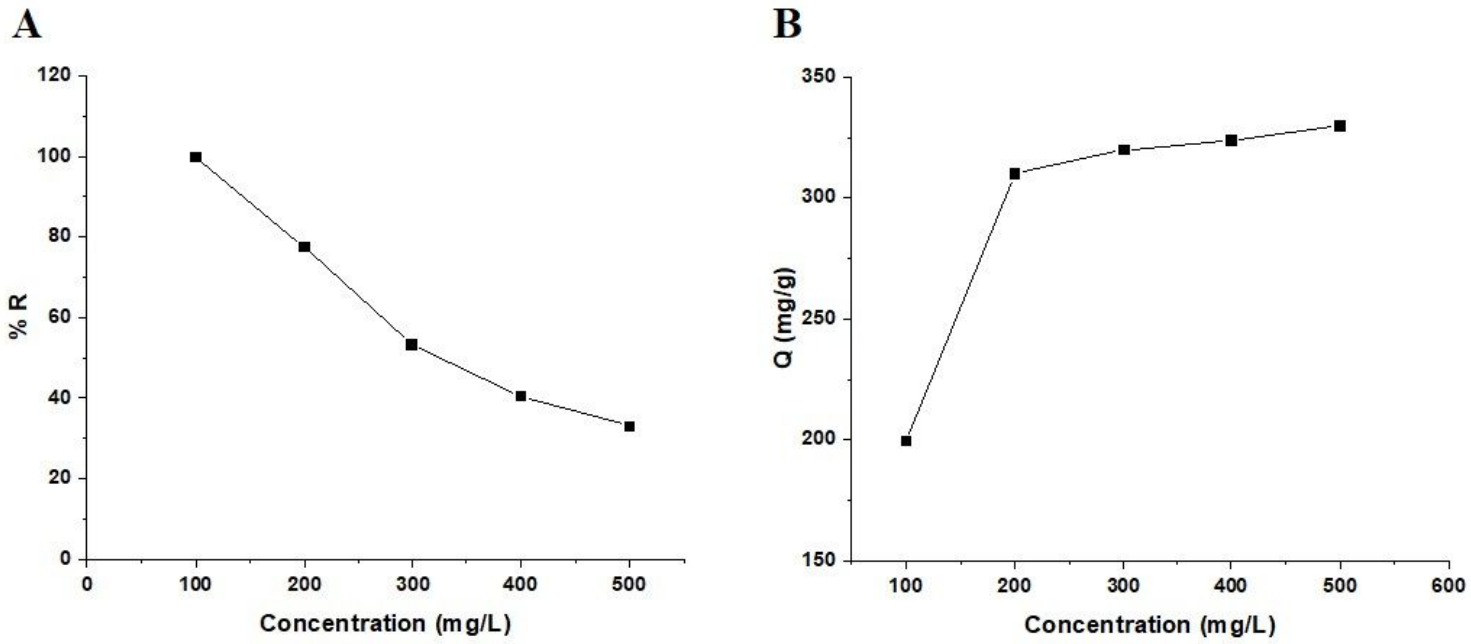

Figure 10

The relation between concentration vs. % removal (A) and capacity (B).

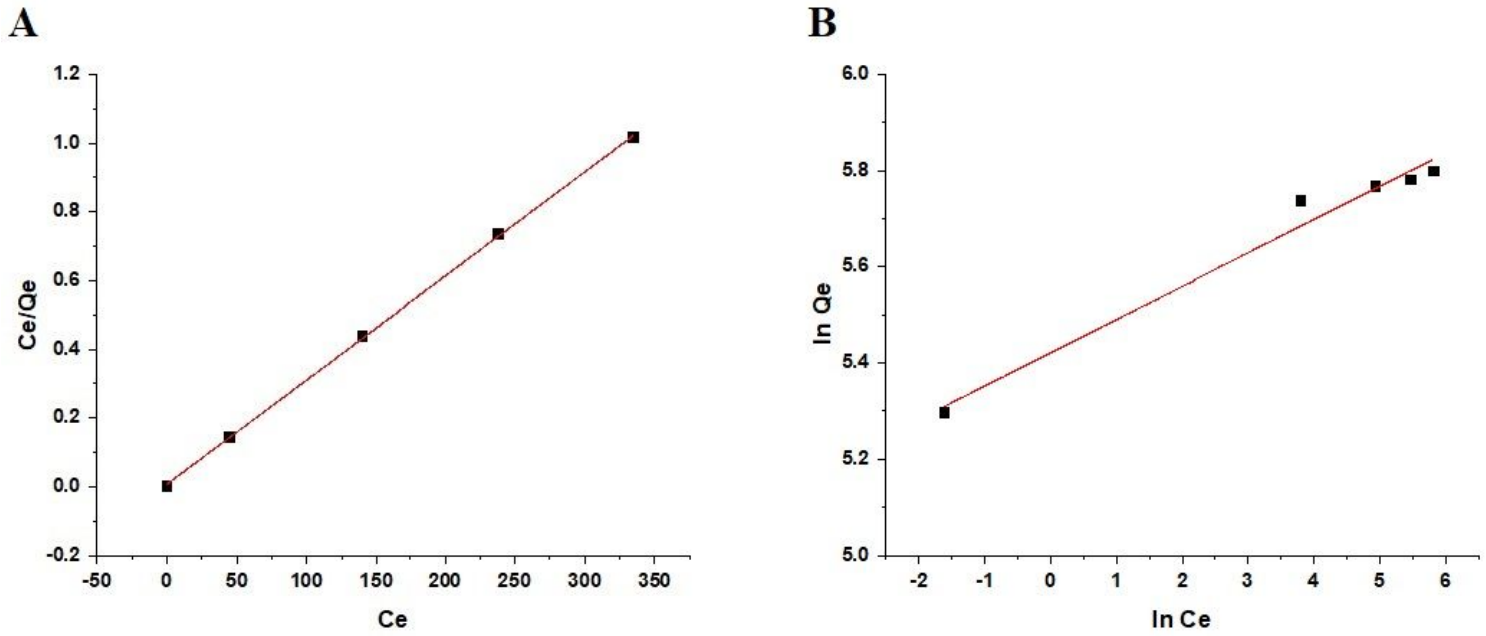

Figure 11

The Langmuir (A) and Freundlich (B) isotherms.

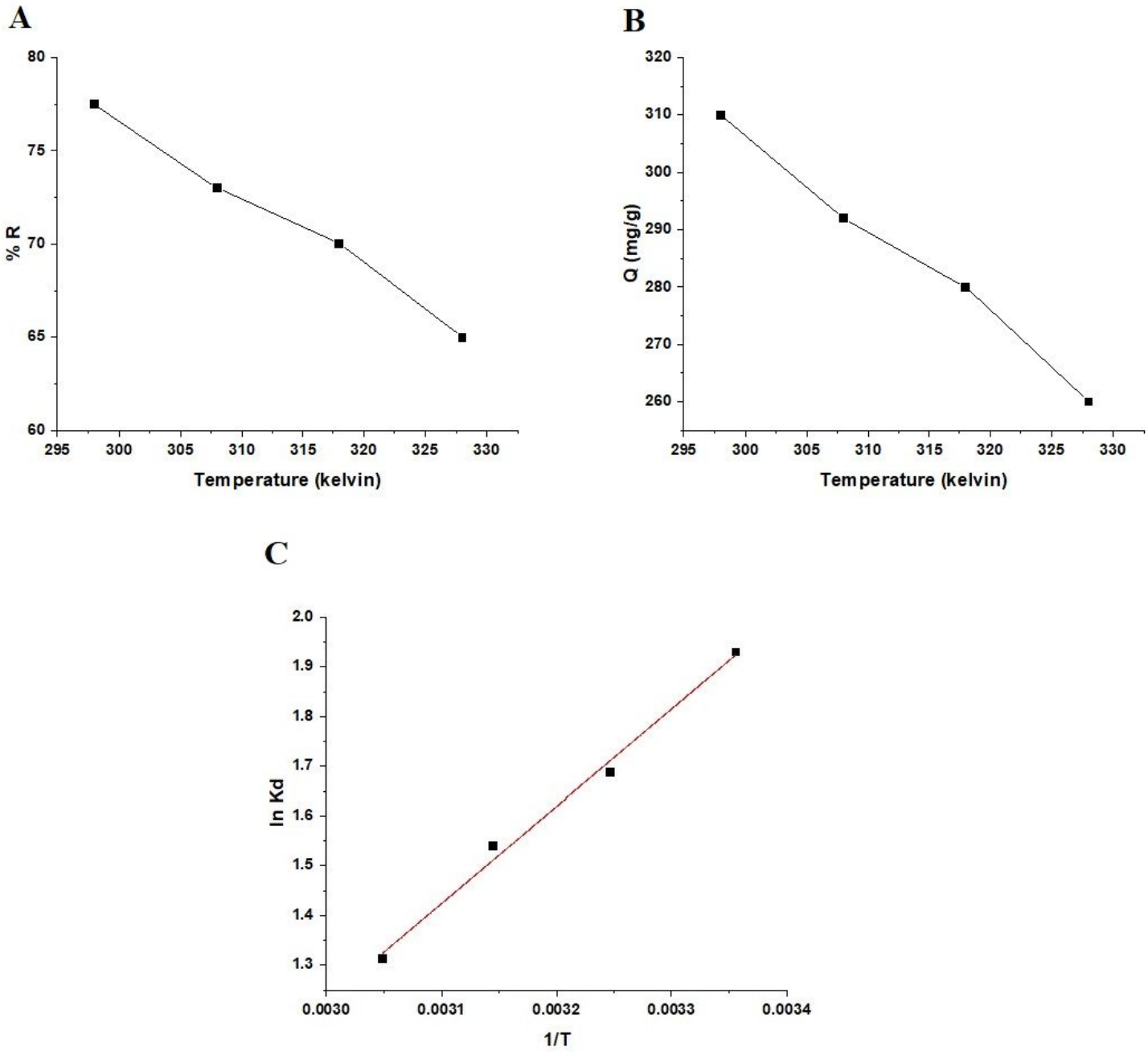

Figure 12

The relation between temperature vs. % removal (A) and capacity (B). The plot of ln Kd vs. 1/T (C).